Journal of The Electrochemical Society, **155** (11) D699-D702 (2008)
0013-4651/2008/155(11)/D699/4/$23.00 © The Electrochemical Society

In Situ Monitoring and Real-Time Control of Gate Hardmask Etching in High-Volume Manufacturing of ICs

Lele Chen,[a,b,z] Weinan Jiang,[c] Todd Pao,[c] Bill Lin,[c] Linda Xu,[c] Gaoming Ji,[c] and Hui Cai[c]

[a]*Shanghai Institute of Microsystem and Information Technology, Chinese Academy of Sciences, Shanghai 200050, China*
[b]*Graduate School, Chinese Academy of Sciences, Beijing 100080, China*
[c]*Grace Semiconductor Manufacturing Corporation, Shanghai, 201203, China*

In the high-volume manufacturing of advanced integrated circuits (ICs), the reproducibility of the gate physical dimension and profile, variation reduction, and control are very important. Continuous running of a gate hardmask etching postprocess switch in fluorocarbon plasma encounters the problems of the gate critical dimension shrinking and the oxide etch rate decreasing as the wafer count increases. To reveal the mechanism and control process shift, optical emission spectroscopy is employed to investigate plasma gas phase and quartz crystal microbalance is employed to investigate real-time polymer deposition on the chamber wall. CF_2 concentration in plasma is found being strong, correlating with the polymer coverage amount on the chamber wall. The mechanism of the plasma-wall interaction is illustrated. The successive decrease of polymer on the chamber wall reduces CF_2 radical density in plasma, which results in gate critical dimension shrinkage and oxide etch rate reduction. The relative CF_2 optical emission intensity is thus proposed to monitor the chamber wall condition and control the gate hardmask critical dimension from run to run to ensure process reproducibility.
 [DOI: 10.1149/1.2971022]

Manuscript submitted April 3, 2008; revised manuscript received July 23, 2008. Published September 9, 2008.

As the semiconductor manufacturing industry moves toward smaller device structures, reproducibility of the device gate critical dimension (CD) becomes a major concern. For better control of CD, dielectric films such as SiO_2, Si_3N_4, or SiON are used as the hardmask layer. Fluorocarbon gas chemistry is usually used to etch hardmask material. One of the sources of the plasma etching process irreproducibility and CD shift is the condition of the chamber wall.

The influence of chamber wall condition on etch process has been observed by many researches previously.[1-4] Schaepkens et al.[1] found that the temperature of the reactor wall has a great effect on gas-phase chemistry and polymer deposition. O'Neill and Singh[2] observed that the presence of polymer films on the wall surface significantly affects the concentration of CF_2 in the discharge using UV absorption spectroscopy. The study carried out by Zhou et al.[4] showed that gas-phase chemistry exhibits different dependence on the wall cleanliness condition. Although many people have stressed the importance of the plasma-wall interaction, its detailed mechanism as well as quantitative analysis has not been well studied.

In this study, it is found that continuous running of the hardmask etching process results in hardmask CD shrinking and the oxide etch rate decreasing as the wafer count increases. During the whole course, all etch parameters, including radio-frequency (rf) power, feed gases, chamber pressure, and cathode temperature, are unchanged. Thus, the primary cause of process shift is the chamber wall condition. This paper will focus on real-time polymer deposition on the chamber wall and its impact on plasma gas phase and, therefore, process shift.

Experimental

The experiment was performed in a parallel-plate reactive ion etching system. The schematic of the experimental reactor was shown in Fig. 1. The power was supplied by a 13.56 MHz rf generator. Four magnetic coils were mounted around the outside of the chamber to create a magnet and enhance plasma density. A 200 mm wafer was placed on a cathode with electrostatic chuck (ESC). In order to maintain good thermal contact between the ESC and the wafer, helium gas at a pressure of 8 Torr was applied to the back side of the wafer. The temperature of the chamber wall was kept at 15°C by means of a chiller. The chamber pressure was controlled by a throttle valve and measured by a capacitance manometer gauge.

Optical emission spectroscopy was used for gas-phase characterization through a quartz window located on the middle of the reactor sidewall. The spectra in the range of 200–800 nm were recorded instantaneously. All species emission intensity used in this paper were normalized to Ar (750 nm) intensity.

A thin-film deposition monitor (Maxtek TM-400) was mounted on the reactor sidewall to monitor real-time polymer deposition. The thin-film deposition monitor was a quartz-crystal microbalance (QCM), which was basically a mass sensing device with excellent resolution and capable of measuring film thickness in real time. The film thickness was calculated by measuring the crystal frequency shift as follows:

$$T_f = \left(\frac{\rho_q}{\rho_f}\right) N_q \left(\frac{\tau}{\pi R_z}\right) \arctan\left[R_z \tan \pi\left(\frac{\tau - \tau_q}{\tau}\right)\right] \qquad [1]$$

where T_f was film thickness, ρ_q was the density of quartz (in grams per cubic centimeter), ρ_f was the density of film, N_q was the frequency constant for an "AT" cut quartz crystal vibrating in thickness shear (in Hertz per centimeter), R_z was the acoustic impedance ratio obtained by dividing the acoustic impedance of quartz by the acoustic impedance of the deposited film, τ_q was the period of uncoated crystal, and τ was the period of the loaded crystal.

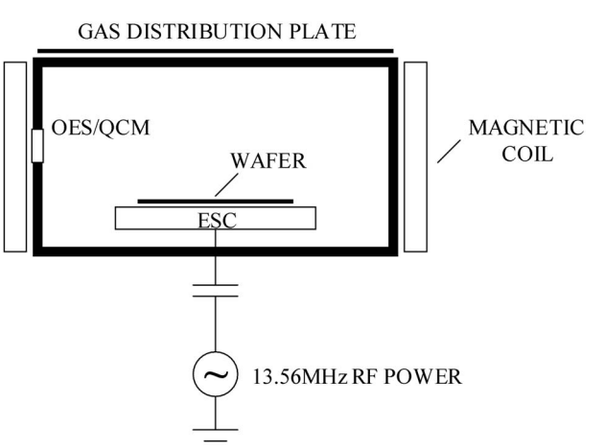

Figure 1. Schematic diagram of the experimental reactor.

[z] E-mail: lelechen@gsmcthw.com

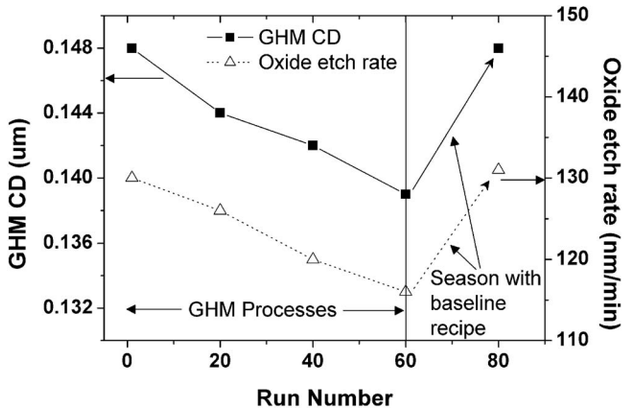

Figure 2. Trends of hard mask CD and oxide etch rate.

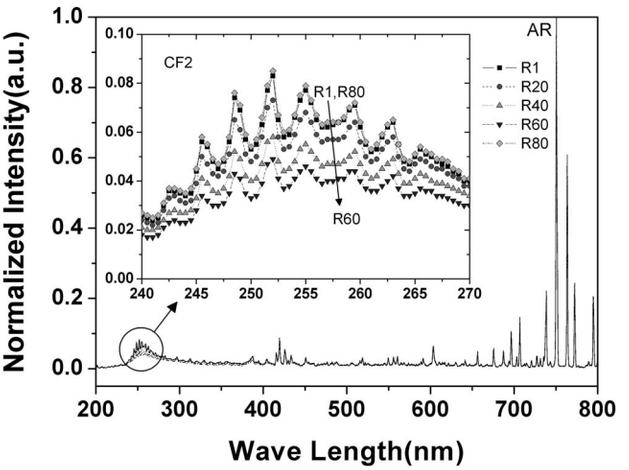

Figure 3. Optical emission spectra of CD samples.

The experimental procedure was carried out as follows. After wet cleaning, the chamber was seasoned with the baseline process (power: 600 W, gas ratio: $CHF_3/CF_4 = 5$, $Ar/CHF_3 + CF_4 = 1.7$, pressure: 120 mTorr, magnet: 30 Gauss). Then, the hardmask process starts (power: 325 W, gas ratio: $CHF_3/CF_4 = 0.7$, $Ar/CHF_3 + CF_4 = 1.5$, O_2: 5 sccm, pressure: 60 mTorr, magnet: 0 Gauss). The hardmask CD and blank oxide etch rate were checked every 20 runs. When the total of 60 runs of the hardmask process finished, the chamber was seasoned with the baseline process once again, and the hardmask CD and oxide etch rate were also checked at the end.

A 1000A blank thermal oxide grown on a silicon substrate was prepared for the etch rate test. Samples for CD test were patterned wafers, which consisted of a photoresist/SiON/SiO_2/Polysilicon/thin oxide/Si substrate stack with a feature size of 0.15 μm. The polysilicon was formed by low-pressure chemical vapor deposition. SiON and SiO_2 were deposited by plasma-enhanced chemical vapor deposition.

Results and Discussion

Trends of gate hardmask CD and oide etch rate.— Figure 2 shows the trends of the hardmask CD and oxide etch rate. With the increase of run number, the hardmask CD reduces from 0.148 to 0.139 μm and the oxide etch rate decreases from 130 to 116 nm/min. After the chamber is seasoned with the baseline process again, the hardmask CD and oxide etch rate come back to the original level. The variation of the hardmask CD and oxide etch rate is up to 12 nm and 12%, respectively.

During the whole course of the experiment, all etch process parameters are kept constant. Thus, the chamber wall condition is the only factor responsible for the etch performance shift. It is suggested that continuous running of the hardmask processes results in a chamber-wall condition shift, which in turn affects the following processes. Seasoning with the baseline process recovers the chamber wall condition then etch performance comes back.

Change of plasma gas phase.— Optical emission spectra of CD samples is shown in Fig. 3. From the wide range of the spectra, the most distinguished area is in the range of 240–270 nm, which corresponds to the CF_2 peaks. It is observed that the intensity of CF_2 peaks decrease with the run number. After the chamber is again seasoned with the baseline process, the intensities come back to the original level. A similar optical emission spectra trend is observed in SiO_2 etch rate tests (not shown).

Other normalized species emission intensities are shown in Fig. 4. All these intensities are normalized to the first sample's intensity. The F (704 nm) intensity keeps almost constant. CF_2 (252 nm) intensity varies significantly. The variation is up to 40%. The trend of SiF (440 nm) intensity is similar to that of CF_2. The other species emission intensity, such as C_2, O, and CO, varies slightly. If we assume that the electron energy distribution function is unchanged in discharge, then the major change of plasma gas phase is the CF_2 radical density.

The relationships between the hardmask CD, oxide etch rate, and CF_2 intensity is shown in Fig. 5. Both hardmask CD and oxide etch rate show strong correlations to CF_2 intensity. Many studies have stressed the importance of CF_x ($x = 1$–3) radicals in the polymer deposition.[5-7] Other groups have also reported strong correlation between the gas phase CF_2 radical concentration and the polymer deposition rate.[8] For the sake of simplicity, the CF_2 density evolution is often used as an indicator of the polymerizing nature of the plasma.[9,10]

During hardmask etching, vertical etching and horizontal etching occurs simultaneously. For hardmask CD, it represents the horizontal etching amount. The polymers deposited on the hardmask lateral sidewall act as an inhibitor to resist horizontal etching. CF_2 radical density in plasma dominates the polymer deposition because the polymer formed on the hardmask sidewall avoids directional ion bombardment, which can remove polymer by physical sputtering. In this case, when CF_2 density decreases in plasma, polymer formed on the hardmask sidewall is reduced, and therefore, horizontal etching is enhanced. As a result, the hardmask CD decreases with CF_2 density.

For a blank oxide etch rate, it represents the vertical etching performance. When the etch starts, a thin fluorocarbon film (<1.5 nm) forms on the oxide surface and is also directly exposed to ion bombardment.[11-13] The dc self-bias voltage is about −410 V

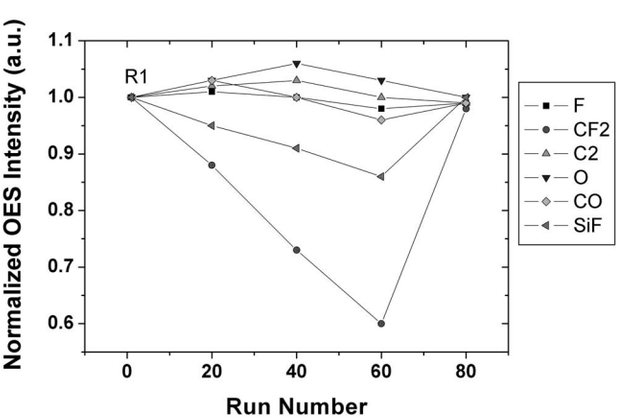

Figure 4. Trends of normalized species emission intensity.

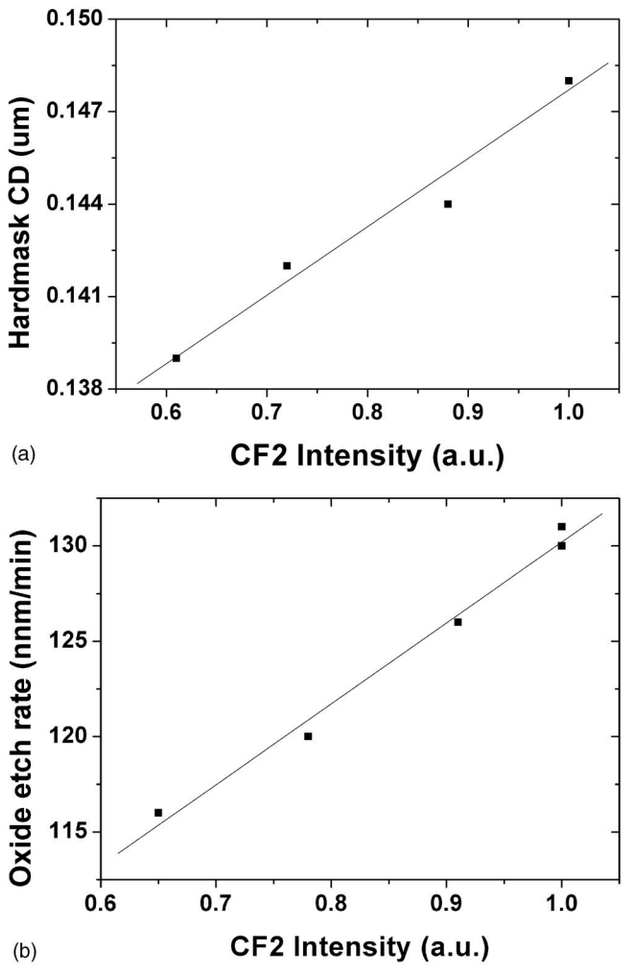

Figure 5. Relationship between (a) hardmask CD, (b) oxide etch rate, and CF_2 intensity.

in our experimental condition. Under this condition, oxide etching is in the regime of ionic and reactive sputtering outlined by Oehrlein et al.[14] At a given power, which means the ion energy is constant, SiO_2 etching is limited by the atomic fluorine provided. Ion-induced defluorination of the fluuorocarbon film can be a main source of fluuorine used for etching of the substrate.[15] When the CF_2 radical reached the oxide surface to form a thin fluorocarbon layer, it is promptly bombarded by high-energy ions and dissociated into CF or C and F radicals, which provide fluorine for oxide etching. When more CF_2 radicals exist in plasma, the SiO_2 etch rate is enhanced because more fluorine sources are provided. In this case, CF_2 is considered as a reactant, which is also proposed by Barela et al.[16] This result is consistent with the observation made by Takada et al., who found a significant contribution of direct SiO_2 etching by fluorocarbon molecules under ion bombardment.[17]

Polymer deposition on the chamber wall.— Figure 6 shows the polymer deposition rate and thickness on the chamber wall during the whole course. The negative deposition rate means the polymer is etched away from the chamber wall. When the chamber is seasoned with a baseline process, polymer rapidly deposits on the chamber wall. The deposition rate is >150 A/min. During the hardmask process, the polymer thickness reduces gradually. The deposition rate is about -37 A/min.

Figure 7 shows the correlation between CF_2 intensity and polymer thickness on the chamber wall. As shown in Fig. 7, CF_2 intensity is directly related to polymer thickness. Thicker polymer on the

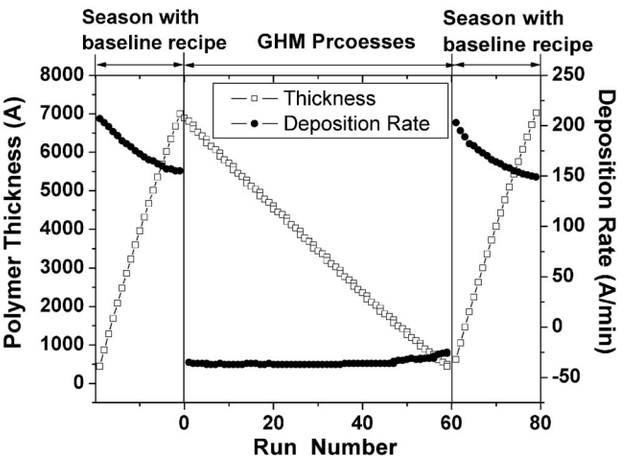

Figure 6. Polymer thickness and deposition rate on chamber wall.

chamber wall produces a higher CF_2 radical density in the plasma. It is suggested that the change of CF_2 radical density in plasma is ascribed to the change of polymer thickness on the chamber wall. Further discussion about the plasma-wall interaction mechanism is presented in the next section.

Two QCM samples are sampled at the highest and lowest CF_2 intensity, respectively. To obtain the polymer composition information, the two samples are examined by ex situ X-ray photoelectron spectroscopy (XPS). The XPS analysis result of C 1s, F 1s, O 1s, and N 1s is shown in Fig. 8. Table I shows the summary of atomic percentages calculated with the atomic sensitivity factor. From the results, it can be found that the main elements of polymer are C and F. Interestingly, the ratio of C/F for both samples is ~ 2. Thus, it can be suggested that the main component of polymer deposited on the chamber wall is poly tetra fluoroethylene-like $(CF_2)_n$.

Plasma-wall interaction mechanism.— In this experiment, two processes are involved. One is the baseline process and the other is the hardmask process. The comparison of the two recipes is shown in Table II. Besides the power, the main differences are feed gases and pressure. The baseline process is of a high CHF_3/CF_4 ratio without O_2, whereas the hardmask process is of a low CHF_3/CF_4 ratio with 5 sccm O_2. The baseline process also has a higher pressure of 120 mTorr, which is twice that of the hardmask process. CHF_3 is well known as a high polymerization gas.[18] O_2 is a primary

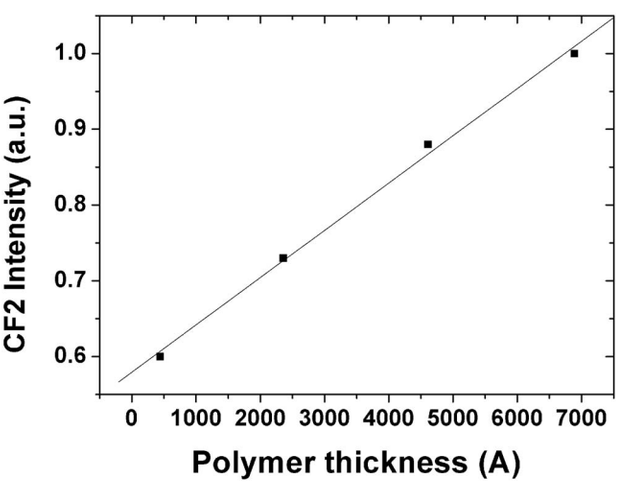

Figure 7. Correlation between CF_2 intensity and polymer thickness.

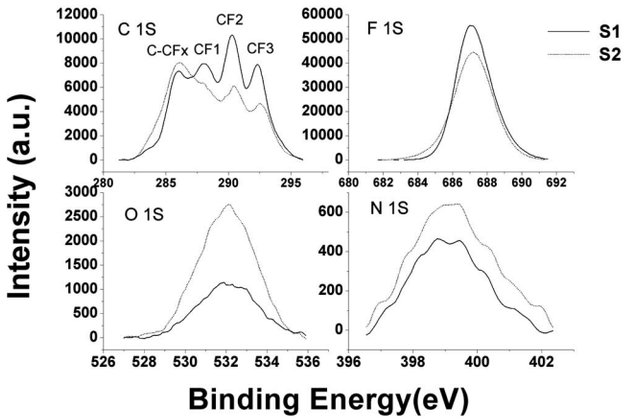

Figure 8. XPS analysis result of QCM samples.

gas to eliminate a carbon-containing polymer precursor and reduce polymer formation by forming volatile CO, CO_2, and COF_2. Higher pressure is in favor of polymerization because of more polymer precursors in plasma. Thus, the baseline process is a high polymerizing process, whereas the hardmask process is a relatively clean process. This is proved by the measurement of QCM.

In fluorocarbon plasma, polymer precursors such as CF_2 and polymer etchants such as F and O coexist in the gas phase. At a given condition, the generation and loss of the polymer precursor and etchant reach a dynamic balance. When the chamber wall is coated with polymer, the polymer on the chamber wall consumes polymer etchants in the plasma. As a result, polymer etchants in the plasma decrease and polymer precursors in the plasma increase. The more polymers that stay on the chamber wall, the more polymer precursors that occur in the plasma. In this case, polymer on the chamber wall is considered as a source of CF_2.

A different type of process results in a different polymer deposition amount on the chamber wall. The recipe detail is determined by the process request. We can eliminate the influence of the chamber wall condition by dedicating the chamber to run each process only. However, the tool capacity utilization and throughput will decrease significantly. For an integrated circuit foundry, exploiting the maximum tool capacity utilization is a high priority. Thus, mixed run and control of process are desired. Results in this paper show that both etch properties and polymer coverage amount on the chamber wall has a good linear relationship with the CF_2 optical emission intensity. Thus, the CF_2 optical emission intensity can be used to monitor the chamber wall condition and control the gate hardmask critical dimension. In practice, when relative CF_2 intensity drops to a critical level, a seasoning with the baseline recipe is implemented to recover the chamber condition. Then, the reproducibility of the process is ensured.

Table I. Summary of atomic percentages.

Atom percent	C 1s	N 1s	O 1s	F 1s	F/C
S1[a]	31.96	1.5	2.34	64.21	2.0
S2[b]	28.22	2.29	6.38	59.3	2.1

[a] S1 is sampled at highest CF_2 intensity.
[b] S2 is sampled at lowest CF_2 intensity.

Table II. Comparison of baseline recipe and hardmask recipe.

Parameter		Baseline	Hardmask
Power (W)		600	325
Pressure (mTorr)		120	60
Gas (sccm)	CHF_3/CF_4	5	0.7
	$Ar/(CHF_3 + CF_4)$	1.7	1.5
	O_2	0	5
Magnet (Gauss)		30	0

Conclusion

The influence of the chamber wall condition on the gate hardmask CD and oxide etch rate is studied in fluorocarbon plasma. Polymer deposition on the chamber wall is an important factor to determining the plasma gas phase and, therefore, etch properties. Polymer on the chamber wall is considered a source of CF_2. Fewer polymers on the chamber wall produce less CF_2 radical in the plasma gas phase, which results in a lower oxide etch rate and smaller critical dimension. The plasma-wall interaction mechanism is also illustrated. Finally, relative CF_2 optical emission intensity is proposed to monitor the chamber wall condition and the control gate hardmask critical dimension from run to run to ensure process reproducibility.

Acknowledgments

The authors acknowledge Dr. Shaohua Liu for useful discussion. The authors also thank Grace Semiconductor Manufacturing Corporation (GSMC) for its support and all etch department colleagues in GSMC for their kind help during the whole study.

References

1. M. Schaepkens, R. C. M. Bosch, T. E. F. M. Standaert, G. S. Oehrlein, and J. M. Cook, *J. Vac. Sci. Technol. A*, **16**, 2099 (1998).
2. J. A. O'Neill and J. Singh, *J. Appl. Phys.*, **77**, 2697 (1995).
3. S. Lee, Y. Tien, and C. Hsu, *Plasma Chem. Plasma Process.*, **19**, 285 (1999).
4. B. Zhou, E. A. Joseph, S. P. Sant, Y. Liu, A. Radhakrishnan, L. J. Overzet, and M. J. Goeckner, *J. Vac. Sci. Technol. A*, **23**, 1657 (2005).
5. J. A. O'Neill and J. Singh, *J. Appl. Phys.*, **77**, 497 (1995).
6. T. Goto and M. Hori, *Jpn. J. Appl. Phys., Part 1*, **35**, 6521 (1996).
7. B. Zhou, E. A. Joseph, L. J. Overzet, and M. J. Goeckner, *J. Vac. Sci. Technol. A*, **24**, 114 (2006).
8. M. M. Millard and E. Kay, *J. Electrochem. Soc.*, **129**, 160 (1982).
9. E. A. Hudson and F. C. Dassapa, *J. Electrochem. Soc.*, **148**, 236 (2001).
10. M. Izawa, 5th International Workshop on Fluorocarbon Plasma, Col de Porte, France (2004).
11. N. R. Rueger, J. J. Beulens, M. Schaepkens, M. F. Doemling, J. M. Mirza, T. E. F. M. Standaert, and G. S. Oehrlein, *J. Vac. Sci. Technol. A*, **15**, 1881 (1997).
12. F. Gaboriau, G. Cartry, M.-C. Peignon, and Ch. Cardinaud, *J. Phys. D*, **39**, 1830 (2006).
13. S. Rauf, T. Sparks, P. L. G. Ventzek, V. V. Smirnov, A. V. Stengach, K. G. Gaynullin, and V. A. Pavlovsky, *J. Appl. Phys.*, **101**, 033308 (2007).
14. G. S. Oehrlein, D. Zhang, D. Vender, and O. Joubert, *J. Vac. Sci. Technol. A*, **12**, 333 (1994).
15. T. E. F. M. Standaert, C. Hedlund, E. A. Joseph, and G. S. Oehrlein, *J. Vac. Sci. Technol. A*, **22**, 53 (2004).
16. M. J. Barela, H. M. Anderson, and G. S. Oehrlein, *J. Vac. Sci. Technol. A*, **23**, 408 (2005).
17. N. Takada, H. Toyoda, I. Murakami, and H. Sugai, *J. Appl. Phys.*, **97**, 013534 (2005).
18. P. J. Astell-Burt, J. A. Cairns, A. K. Cheetham, and R. M. Hazel, *Plasma Chem. Plasma Process.*, **6**, 417 (1986).